

# Learning Multiscale Consistency for Self-supervised Electron Microscopy Instance Segmentation

Yinda Chen, Wei Huang, Xiaoyu Liu, Qi Chen, Zhiwei Xiong

University of Science and Technology of China

**Abstract.** Instance segmentation in electron microscopy (EM) volumes poses a significant challenge due to the complex morphology of instances and insufficient annotations. Self-supervised learning has recently emerged as a promising solution, enabling the acquisition of prior knowledge of cellular tissue structures that are essential for EM instance segmentation. However, existing pretraining methods often lack the ability to capture complex visual patterns and relationships between voxels, which results in the acquired prior knowledge being insufficient for downstream EM analysis tasks. In this paper, we propose a novel pretraining framework that leverages multiscale visual representations to capture both voxel-level and feature-level consistency in EM volumes. Specifically, our framework enforces voxel-level consistency between the outputs of a Siamese network by a reconstruction function, and incorporates a cross-attention mechanism for soft feature matching to achieve fine-grained feature-level consistency. Moreover, we propose a contrastive learning scheme on the feature pyramid to extract discriminative features across multiple scales. We extensively pretrain our method on four large-scale EM datasets, achieving promising performance improvements in representative tasks of neuron and mitochondria instance segmentation.

**Keywords:** Self-supervised pretraining · Instance segmentation · Electron microscopy volume.

## 1 Introduction

Electron microscopy (EM) imaging plays a vital role in providing high-resolution views of cellular tissue structures, especially in the nervous system [22]. With the development of deep learning techniques, automatic segmentation for EM volumes has become an indispensable tool for analyzing the huge amount data [2,10,17,18]. However, existing fully supervised EM instance segmentation methods are fragile due to a lack of sufficient annotations [13].

Self-supervised learning exploits the inherent structure and information within data to acquire meaningful representations without the supervision of manual annotations, which brings performance improvement in downstream tasks [3,12]. However, existing self-supervised pretraining methods often rely on simple and

generic proxy tasks, such as image reconstruction [7,28,5], which cannot fully exploit the complex and diverse visual representations in EM volumes.

To address this issue, we propose a multiscale consistency pretraining framework tailored for EM volumes. The framework focuses on learning visual representation consistency at different scales through joint training on multiple tasks, including voxel-level reconstruction, soft feature matching, and feature contrastive learning. To obtain robust EM visual representations, we utilize a Siamese network architecture with a CNN or Transformer backbone to extract features from strongly and weakly augmented EM volume inputs. To maintain voxel-level consistency in the latent representations, we first enforce the network to reconstruct the original volume from its augmented counterparts. To achieve fine-grained feature-level consistency, we then adopt a cross-attention mechanism for soft feature matching between strong and weak augmentations. Moreover, we propose a contrastive learning scheme on the feature pyramid, which utilizes a hierarchical approach to compute similarity scores across different levels of the pyramid. In this way, we promote the network to learn invariant features on multiple scales, thereby enhancing its robustness to complex instance morphology in EM volumes.

Our contributions are as follows: 1) We propose a novel framework tailored for EM volume pretraining, enforcing both voxel-level and feature-level consistency in EM visual representations. 2) We utilize a Siamese network with cross-attention to focus on features at different scales for fine-grained feature matching. 3) We conduct extensive pretraining on four large-scale EM datasets using both CNN and Transformer backbones and demonstrate the effectiveness of our framework on downstream tasks of neuron segmentation and mitochondria segmentation.

## 2 Methodology

### 2.1 Siamese Network Design

To enhance the robustness of the network and improve its ability to extract features at different scales, we feed both strongly augmented and weakly augmented data into a Siamese network as shown in Figure 1(a). Strong augmentation techniques include elastic deformation, Gaussian noise, gamma transformation, cropping, splicing, scaling, and large-scale masking, while weak augmentation techniques consist of simple transformations such as translation, rotation, scaling, and flipping. We transform the original 3D pretraining data  $\mathcal{D}$  into  $\mathcal{D}' = \{(x_{w,1}, x_{s,1}), (x_{w,2}, x_{s,2}), \dots, (x_{w,N}, x_{s,N})\}$ , where  $x_{w,i}, x_{s,i}$  represent the weakly and strongly augmented inputs, respectively, with  $x_{w,i}, x_{s,i} \in \mathbb{R}^{B \times C \times H \times W \times D}$ . Here,  $B$  represents the batch size,  $C$  represents the number of channels, and  $H, W, D$  represent the dimensions of the volume. The transformed data are then mapped into the latent space using a shared-weight backbone, such as UNet or ViT, to generate features at different scales. For example, given  $x_{w,1}$  as input, the decoder of our main network generates a series of encoded visual features  $\mathbf{W}_1 = \{\mathbf{w}_1^1, \mathbf{w}_1^2, \dots, \mathbf{w}_1^N, \mathbf{w}_1^{out}\}$ , where  $\mathbf{w}_i^j \in \mathbb{R}^{B \times C_1 \times H_1 \times W_1 \times D_1}$ . Note that the output features have a high dimension  $C_i$ , which can lead to increased

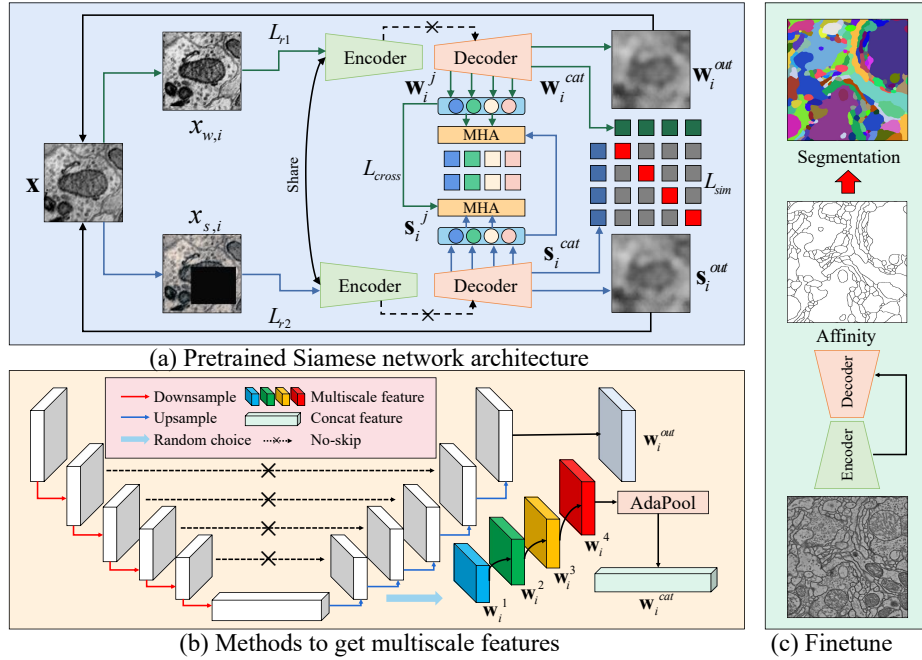


**Fig. 1.** Our proposed method consists of two stages: pretraining and finetuning. (a) illustrates the framework of pretraining, which aims to add consistency constraints to both weakly and strongly augmented data. (b) describes the method to extract multiscale features. (c) outlines our instance segmentation method during the finetuning stage.

computational complexity. To mitigate this issue, we introduce a random factor  $C'_i = \lambda C_i$  and set a smaller value of  $\lambda$  for features with higher dimensions. To ensure consistent output sizes, we pass the multiscale features through an Adaptive Average Pooling layer, resulting in encoded features with dimensions of  $H_i = 16, W_i = 16, D_i = 16$ . Moreover, we eliminate the skip connections in the UNet structure to stop the network from producing degenerate solutions based on input features from the encoder [27].

## 2.2 Pretraining Method

**Voxel-level Reconstruction.** Self-supervised reconstruction tasks can be used to learn visual representations with good reconstruction performance [13]. By embedding input data into a high-dimensional space and then reconstructing it back to the original input, the model can learn a robust representation of the input data. Therefore, we added a consistency reconstruction objective to the output of the Siamese network, aimed at reconstructing the original input under strong and weak data augmentation. The loss function of the reconstruction task can be formulated as follows:

$$L_r = \frac{1}{2N} \sum_{i=1}^N (\|\mathbf{w}_i^{out} - \mathbf{x}_i\|_2^2 + \|\mathbf{s}_i^{out} - \mathbf{x}_i\|_2^2). \quad (1)$$

**Soft Feature Matching based on Cross-attention.** Cross-attention based feature match does not require explicit feature extraction and handles larger variations between input data [24]. Since our Siamese network introduces complex deformations and perturbations, we introduce a bidirectional cross-attention mechanism to match fine-grained features. The specific technical details are as follows.

For each pair of strong-weak augmentation  $(\mathbf{W}_i, \mathbf{S}_i)$ , we first project them into lower-dimensional embeddings using  $\mathbf{W}_i = MLP(\mathbf{w}_i^1, \mathbf{w}_i^2, \dots, \mathbf{w}_i^N)$  and  $\mathbf{S}_i = MLP(\mathbf{s}_i^1, \mathbf{s}_i^2, \dots, \mathbf{s}_i^N)$ . To enhance the correlation between strong and weak augmentation tokens, we propose to utilize a cross-attention mechanism [15] to compute soft feature matching between generated strong-weak augmentation tokens. Specifically, for the  $j$ -th strong augmentation token embedding  $\mathbf{w}_i^j$  in the  $i$ -th strong-weak augmentation pair, we let  $\mathbf{w}_i^j$  attend to all weak augmentation token embeddings in  $\mathbf{S}_i$ . We first compute bidirectional cross-attention:

$$v_i^{j2k} = \text{softmax} \left[ \frac{(Q\mathbf{w}_i^j)^T (K\mathbf{s}_i^k)}{\sqrt{d}} \right], \omega_i^{j2k} = \text{softmax} \left[ \frac{(Q\mathbf{s}_i^j)^T (K\mathbf{w}_i^k)}{\sqrt{d}} \right], \quad (2)$$

and then calculate their attention weights  $\mathbf{m}_i^j = \sum_{k=1}^N [v_i^{j2k} (V\mathbf{s}_i^k)]$  and  $\mathbf{n}_i^j = \sum_{k=1}^N [\omega_i^{j2k} (V\mathbf{w}_i^k)]$ , where K, Q, and V are learnable matrices. We introduce InfoNCE loss [12] to pull the corresponding strong-weak token embeddings closer but push them away from other token embeddings, and the resulting cross-attention loss is calculated as follows:

$$L_{cross} = -\frac{1}{NB} \sum_{i=1}^N \sum_{j=1}^B \text{InfoNCE} < (\mathbf{m}_i^j, \mathbf{n}_i^j) / \tau_1 >, \quad (3)$$

where  $\tau_1$  is the temperature hyperparameter.

**Multiscale Feature Contrastive Learning.** Generally, common SSL algorithms only consider the final outputs  $\mathbf{w}_i^{out}$  and  $\mathbf{s}_i^{out}$  of the Siamese network and minimize the distance between them [4,26,6]. Although this method is computationally efficient, it overlooks the importance of multiscale features in EM volumes and poses challenges in network training. Inspired by [27,19], we adopt a Siamese learning method with multiscale comparisons for SSL, where we minimize the distances between each feature pair  $\mathbf{w}_i^j$  and  $\mathbf{s}_i^j$  at different scales, forcing the model to retain multiscale self-supervised representations as shown in Figure 1(b).

For a given feature pair  $(\mathbf{w}_i^j, \mathbf{s}_i^j)$ , we first randomly select  $\lambda_i C_i$  channels from each feature. We then normalize the size of the features using Adaptive Average Pooling, concatenate the features from different layers to obtain  $\mathbf{w}_i^{cat}$  and  $\mathbf{s}_i^{cat}$ , and flatten the concatenated features to compute their similarity. The dimension of the output vector  $f(\mathbf{w}_i^{cat})$  and  $f(\mathbf{s}_i^{cat})$  is  $B \times C_{cat} \times (D_i H_i L_i)$ . We then calculate the similarity of the multiscale features of the Siamese network using cosine similarity. We compute the multiscale similarity loss  $L_{sim}$  for the entire batch as follows:

$$L_{sim} = -\log \frac{\exp[\cos \langle f(\mathbf{w}_i^{cat}), f(\mathbf{s}_i^{cat}) \rangle / \tau_2]}{\sum_{i=1}^B \exp[\cos \langle f(\mathbf{w}_i^{cat}), f(\mathbf{s}_i^{cat}) \rangle / \tau_2]}, \quad (4)$$

where  $\tau_2$  is the temperature hyperparameter and  $B$  is the total batch size.

Our pretraining method’s loss function is mainly composed of the three aforementioned parts. Therefore, the final loss function can be described as follows:

$$L_{total} = \alpha_1 L_r + \alpha_2 L_{cross} + \alpha_3 L_{sim}, \quad (5)$$

where  $\alpha_1$ ,  $\alpha_2$ , and  $\alpha_3$  represent weighting coefficients.

### 3 Experiments and Results

**Dataset.** Our pretraining data consists of four large-scale EM datasets, *i.e.*, the Full Adult Fly Brain (FAFB) [21], MitoEM [25], FIB-25 [23], and Kasthuri15 [16] datasets. They are imaged from different organisms, including *Drosophila*, mouse, rat, and human. To ensure balance and diversity in the data fed into the network, we uniformly sample from these four datasets with equal probabilities for each batch input. where MitoEM contains two volumes, *i.e.*, MitoEM-H and MitoEM-R Our pretraining data comprises four large-scale EM datasets. The Full Adult Fly Brain (FAFB) [21] consists of 7062 sections of EM volumes with a resolution of  $286720 \times 155648$  pixels acquired using serial section transmission EM. MitoEM-H and MitoEM-R [25] are 3D mitochondria instance segmentation datasets with a volume of  $30 \mu m^3$  from the human and rat cortex. The FIB-25 [23] dataset comprises a  $5 \times 5 \times 5 \mu m$  section from the CA1 hippocampus region of the brain, corresponding to a  $1065 \times 2048 \times 1536$  volume with a resolution of approximately  $5 \times 5 \times 5 nm$  per voxel. The Kasthuri15 [16] dataset is a large-scale EM dataset of mouse neocortex acquired by serial section EM, covering an area of about  $1500 \times 1500 \times 185$  microns at a resolution of approximately  $3 \times 3 \times 30 nm$  per voxel. To ensure balance and diversity in the data fed into the network, we uniformly sample from these four datasets with equal probabilities for each batch input to the dataloader.

To validate the effectiveness of our pretraining method, we conduct experiments for neuron and mitochondria segmentation tasks in the finetuning stage. For neuron segmentation, we utilize the AC3/AC4 [16], CREMI A/B/C datasets [9], training on 75 or 25 of the images and testing on the remaining 50 images.

**Table 1.** Quantitative comparisons for neuron segmentation on the AC4 and CREMI datasets.

Dataset	Method	75-train, 50-test				25-train, 50-test			
		waterz		LMC		waterz		LMC	
		VOI ↓	Arand ↓	VOI ↓	Arand ↓	VOI ↓	Arand ↓	VOI ↓	Arand ↓
AC4	MALA [10]	1.214	0.301	1.270	0.164	1.459	0.198	1.268	0.131
	UNETR [11]	1.357	0.308	1.659	0.199	2.239	0.387	2.439	0.367
	Superhuman [17]	0.978	0.230	1.174	0.110	1.127	0.256	1.171	0.146
	PEA [14]	0.900	<b>0.145</b>	1.096	<b>0.088</b>	1.063	<b>0.115</b>	1.125	0.128
	ours+MALA	1.093	0.233	1.218	0.114	1.288	0.168	1.241	<b>0.118</b>
	ours+UNETR	1.329	0.270	1.619	0.201	1.837	0.309	2.227	0.336
	ours+Superhuman	<b>0.826</b>	0.184	<b>1.084</b>	0.105	<b>0.900</b>	0.197	<b>1.115</b>	0.120
CREMI	MALA [10]	1.418	0.217	1.320	0.132	1.565	0.248	1.482	0.153
	UNETR [11]	1.282	0.184	1.442	0.142	1.419	0.172	1.517	0.154
	Superhuman [17]	1.106	0.108	1.189	0.109	1.403	0.194	1.399	0.137
	PEA [14]	1.158	0.147	1.137	0.108	1.381	0.175	1.293	0.124
	ours+MALA	1.293	0.184	1.219	0.117	1.313	0.195	1.278	0.133
	ours+UNETR	1.189	0.170	1.405	0.138	1.273	0.160	1.427	0.138
	ours+Superhuman	<b>1.024</b>	<b>0.107</b>	<b>1.118</b>	<b>0.106</b>	<b>1.168</b>	<b>0.154</b>	<b>1.210</b>	<b>0.115</b>

For the mitochondria segmentation task, we adopt the MitoEM-R dataset [25], training on the first 400 or 100 images and testing on the remaining 100 images.

**Evaluation Metrics and Hyperparameters.** In the finetuning stage, we evaluate our pretraining method on two 3D instance segmentation tasks: neuron segmentation and mitochondria segmentation. As illustrated in Figure 1(c), following [14,18], we predict the instance’s affinity map or boundary map through the network and generate specific instances via post-processing methods like LMC [2] and waterz [10]. We load the weights obtained from pretraining to improve the final instance segmentation performance and demonstrate the effectiveness of our pretraining method.

For neuron instance segmentation, we evaluate performance using the Variation of Information (VOI) [20] and Adapted Rand (Arand) [1] metrics, while for mitochondria segmentation, we use the average precision with an IoU threshold of 0.75 (AP75) metric. Additionally, following [25], we provide evaluation metrics for different sizes of mitochondria instances based on the number of mitochondria voxels, with thresholds set at 5K and 15K for small, medium, and large instances, respectively.

We employ the Adam optimizer with  $\beta_1 = 0.9, \beta_2 = 0.999$  and set the learning rate to  $1 \times 10^{-4}$  for both pretraining and finetuning. Pretraining is conducted with a batch size of 8 on 4 NVIDIA RTX 3090s GPUs. We randomly sample the four large-scale EM datasets with equal probability and train the network for a total of 500K iterations. In the finetuning phase, we set the batch size to 4 on 2 NVIDIA RTX 3090s GPUs, and conduct experiments on both neuron and mitochondria segmentation tasks, with 200K iterations for each task.

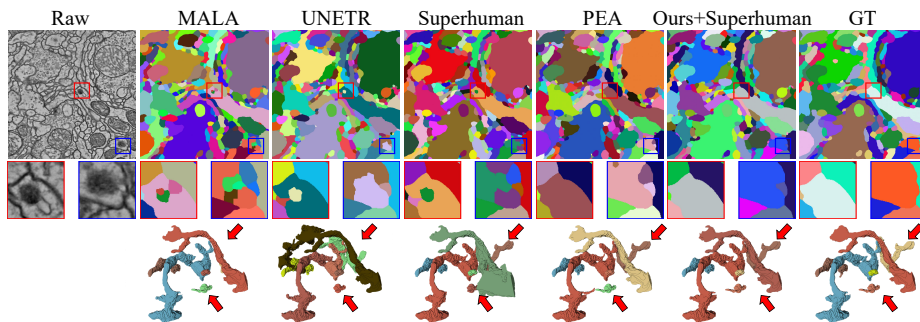


**Fig. 2.** Visual comparisons for neuron segmentation, where colored boxes and arrows highlight the significant differences in 2D and 3D segmentation results, respectively.

**Neuron Segmentation.** We replicate three CNN architectures, Superhuman [17], MALA [10], and PEA [14], as well as one transformer-based architecture UNETR [11], on the AC3/AC4 and CREMI datasets. The segmentation performance for neuron detection is presented in Table 1. Visualization results can be seen in Figure 2.

Our experimental results demonstrate that our method provides promising gains across different backbones, with the CREMI results representing an average on the CREMI A/B/C datasets. We observe that our pretraining method is particularly advantageous for a small amount of finetuning data. For example, when using the waterz method for post-processing, the VOI gain averages 10.5% for finetuning with 75 images, while the VOI gain reaches 20.1% for finetuning with only 25 images, even surpassing the results obtained by direct training on 75 images. This indicates that our method is particularly effective for scenarios with limited annotation resources.

**Mitochondria Segmentation.** We evaluate the effectiveness of our method on mitochondria segmentation using the MitoEM-R dataset. We reproduce four networks, including UNet++ [29], UNETR [11], ResUnet [8], and Res-Unet-R [18]. We finetune these models on the first 400/100 images, respectively, and test them on the last 100 images. We present the mitochondria segmentation results in Table 2, and detailed visualizations are shown in Figure 3.

Our experimental results demonstrate that our method achieves comparable results to the current SOTA [18] when finetuning with 400 images for mitochondria segmentation. Furthermore, we observe a 37.0% improvement in AP75 on difficult instances, i.e., small volume mitochondria segmentation, indicating that our pretraining method greatly enhances segmentation performance on challenging examples. Additionally, in the experimental design where only 1/4 of the data are used for finetuning, our method achieves results almost identical to those obtained by finetuning the full dataset. This suggests that our pretraining method has great potential for improving segmentation performance on difficult samples.

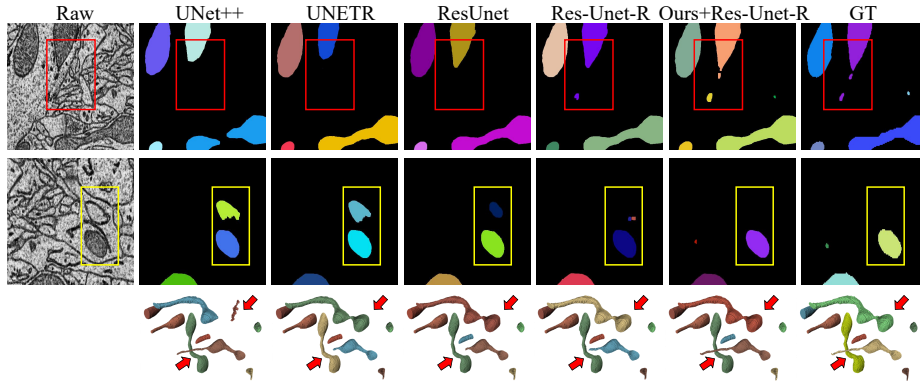


**Fig. 3.** Visual comparisons for mitochondria segmentation, where colored boxes and arrows highlight the significant differences in 2D and 3D segmentation results, respectively.

**Table 2.** Quantitative comparisons for mitochondria segmentation on the MitoEM-R dataset.

Methods	AP-75 (400-train,100-test)				AP-75 (100-train,100-test)			
	All $\uparrow$	small $\uparrow$	medium $\uparrow$	large $\uparrow$	All $\uparrow$	small $\uparrow$	medium $\uparrow$	large $\uparrow$
UNet++ [29]	0.845	0.240	0.832	0.870	0.788	0.212	0.796	0.813
UNETR [11]	0.861	0.294	0.847	0.886	0.822	0.255	0.811	0.833
ResUnet [8]	0.884	0.375	0.860	0.901	0.854	0.322	0.843	0.876
Res-UNet-R [18]	<b>0.904</b>	0.303	0.841	<b>0.934</b>	0.882	0.296	0.831	0.891
Ours+Res-UNet-R	0.901	<b>0.415</b>	<b>0.878</b>	0.921	<b>0.896</b>	<b>0.401</b>	<b>0.872</b>	<b>0.917</b>

**Ablation Study.** We present ablation experimental results on the multi-task constraints as shown in Table 3, with additional ablation experiments available in the supplementary material. Specifically, we finetuned our model using the first 25 images of the CREMI C dataset with a Superhuman backbone and observed a maximum improvement of 34.26% in performance compared to the baseline method. Additionally, we found that the soft feature matching in the cross-attention mechanism and the reconstruction task have promising improvements in downstream segmentation performance.

**Table 3.** Ablation study on the multi-task pretraining.

Dataset	$L_{sim}$	$L_r$	$L_{cross}$	VOI $\downarrow$	Arand $\downarrow$
				1.924	0.192
CREMI C			✓	1.779(+0.145)	0.204(-0.012)
		✓		1.601(+0.323)	0.178(+0.014)
		✓	✓	1.444(+0.480)	<b>0.153(+0.039)</b>
	✓	✓	✓	<b>1.433(+0.491)</b>	0.162(+0.030)

## 4 Conclusion

In this paper, we propose a novel pretraining framework for EM volumes that leverages voxel-level reconstruction, soft feature matching based on cross-attention, and multiscale feature contrastive learning. By imposing consistent output constraints on the strong-weak data augmentation inputs of a Siamese network, our framework preserves both voxel-level and feature-level consistency in the latent representations of EM volumes. We pretrain our model on four large-scale EM datasets to ensure data diversity and balance. Compared to existing methods based on either CNN or Transformer, our framework demonstrates promising performance improvements in neuron and mitochondria instance segmentation with complex instance morphology and insufficient annotations.

## References

1. Ignacio Arganda-Carreras, Srinivas C Turaga, Daniel R Berger, Dan Cireşan, Alessandro Giusti, Luca M Gambardella, Jürgen Schmidhuber, Dmitry Laptev, Sarvesh Dwivedi, Joachim M Buhmann, et al. Crowdsourcing the creation of image segmentation algorithms for connectomics. *Frontiers in neuroanatomy*, page 142, 2015.
2. Thorsten Beier, Constantin Pape, Nasim Rahaman, Timo Prange, Stuart Berg, Davi D Bock, Albert Cardona, Graham W Knott, Stephen M Plaza, Louis K Scheffer, et al. Multicut brings automated neurite segmentation closer to human performance. *Nature methods*, 14(2):101–102, 2017.
3. Ting Chen, Simon Kornblith, Mohammad Norouzi, and Geoffrey Hinton. A simple framework for contrastive learning of visual representations. In *International conference on machine learning*, pages 1597–1607. PMLR, 2020.
4. Xinlei Chen, Haoqi Fan, Ross Girshick, and Kaiming He. Improved baselines with momentum contrastive learning. *arXiv preprint arXiv:2003.04297*, 2020.
5. Yinda Chen, Wei Huang, Shenglong Zhou, Qi Chen, and Zhiwei Xiong. Self-supervised neuron segmentation with multi-agent reinforcement learning. In *IJCAI*, 2023.
6. Yinda Chen, Che Liu, Wei Huang, Sibio Cheng, Rossella Arcucci, and Zhiwei Xiong. Generative text-guided 3d vision-language pretraining for unified medical image segmentation. *arXiv preprint arXiv:2306.04811*, 2023.
7. Zhihong Chen, Yuhao Du, Jinpeng Hu, Yang Liu, Guanbin Li, Xiang Wan, and Tsung-Hui Chang. Multi-modal masked autoencoders for medical vision-and-language pre-training. In *Medical Image Computing and Computer Assisted Intervention–MICCAI 2022: 25th International Conference, Singapore, September 18–22, 2022, Proceedings, Part V*, pages 679–689. Springer, 2022.
8. Foivos I Diakogiannis, François Waldner, Peter Caccetta, and Chen Wu. Resunet-a: A deep learning framework for semantic segmentation of remotely sensed data. *ISPRS Journal of Photogrammetry and Remote Sensing*, 162:94–114, 2020.
9. J Funke, S Saalfeld, DD Bock, SC Turaga, and E Perlman. Miccai challenge on circuit reconstruction from electron microscopy images, 2016.
10. Jan Funke, Fabian Tschopp, William Grisaitis, Arlo Sheridan, Chandan Singh, Stephan Saalfeld, and Srinivas C Turaga. Large scale image segmentation with structured loss based deep learning for connectome reconstruction. *IEEE transactions on pattern analysis and machine intelligence*, 41(7):1669–1680, 2018.

11. Ali Hatamizadeh, Yucheng Tang, Vishwesh Nath, Dong Yang, Andriy Myronenko, Bennett Landman, Holger R Roth, and Daguang Xu. Unetr: Transformers for 3d medical image segmentation. In *Proceedings of the IEEE/CVF winter conference on applications of computer vision*, pages 574–584, 2022.
12. Kaiming He, Haoqi Fan, Yuxin Wu, Saining Xie, and Ross Girshick. Momentum contrast for unsupervised visual representation learning. In *Proceedings of the IEEE/CVF conference on computer vision and pattern recognition*, pages 9729–9738, 2020.
13. Wei Huang, Chang Chen, Zhiwei Xiong, Yueyi Zhang, Xuejin Chen, Xiaoyan Sun, and Feng Wu. Semi-supervised neuron segmentation via reinforced consistency learning. *IEEE Transactions on Medical Imaging*, 41(11):3016–3028, 2022.
14. Wei Huang, Shiyu Deng, Chang Chen, Xueyang Fu, and Zhiwei Xiong. Learning to model pixel-embedded affinity for homogeneous instance segmentation. In *Proceedings of the AAAI Conference on Artificial Intelligence*, volume 36, pages 1007–1015, 2022.
15. Zilong Huang, Xinggang Wang, Lichao Huang, Chang Huang, Yunchao Wei, and Wenyu Liu. Ccnet: Criss-cross attention for semantic segmentation. In *Proceedings of the IEEE/CVF international conference on computer vision*, pages 603–612, 2019.
16. Narayanan Kasthuri, Kenneth Jeffrey Hayworth, Daniel Raimund Berger, Richard Lee Schalek, José Angel Conchello, Seymour Knowles-Barley, Dongil Lee, Amelio Vázquez-Reina, Verena Kaynig, Thouis Raymond Jones, et al. Saturated reconstruction of a volume of neocortex. *Cell*, 162(3):648–661, 2015.
17. Kisuk Lee, Jonathan Zung, Peter Li, Viren Jain, and H Sebastian Seung. Superhuman accuracy on the snemi3d connectomics challenge. *arXiv preprint arXiv:1706.00120*, 2017.
18. Mingxing Li, Chang Chen, Xiaoyu Liu, Wei Huang, Yueyi Zhang, and Zhiwei Xiong. Advanced deep networks for 3d mitochondria instance segmentation. In *2022 IEEE 19th International Symposium on Biomedical Imaging (ISBI)*, pages 1–5. IEEE, 2022.
19. Shentong Mo, Zhun Sun, and Chao Li. Multi-level contrastive learning for self-supervised vision transformers. In *Proceedings of the IEEE/CVF Winter Conference on Applications of Computer Vision*, pages 2778–2787, 2023.
20. Juan Nunez-Iglesias, Ryan Kennedy, Toufiq Parag, Jianbo Shi, and Dmitri B Chklovskii. Machine learning of hierarchical clustering to segment 2d and 3d images. *PloS one*, 8(8):e71715, 2013.
21. Philipp Schlegel, Alexander S Bates, Tejal Parag, Gregory SXE Jefferis, and Davi D Bock. Automatic detection of synaptic partners in a whole-brain drosophila em dataset. *Nature Methods*, 18(8):877–884, 2021.
22. Arlo Sheridan, Tri M Nguyen, Diptodip Deb, Wei-Chung Allen Lee, Stephan Saalfeld, Srinivas C Turaga, Uri Manor, and Jan Funke. Local shape descriptors for neuron segmentation. *Nature Methods*, pages 1–9, 2022.
23. Shin-ya Takemura, Yoshinori Aso, Toshihide Hige, Allan Wong, Zhiyuan Lu, C Shan Xu, Patricia K Rivlin, Harald Hess, Ting Zhao, Toufiq Parag, et al. A connectome of a learning and memory center in the adult drosophila brain. *Elife*, 6:e26975, 2017.
24. Fuying Wang, Yuyin Zhou, Shujun Wang, Varut Vardhanabhuti, and Lequan Yu. Multi-granularity cross-modal alignment for generalized medical visual representation learning. In *Advances in Neural Information Processing Systems*, 2022.

25. Donglai Wei, Zudi Lin, Daniel Franco-Barranco, Nils Wendt, Xingyu Liu, Wenjie Yin, Xin Huang, Aarush Gupta, Won-Dong Jang, Xueying Wang, et al. Mitoem dataset: Large-scale 3d mitochondria instance segmentation from em images. In *International Conference on Medical Image Computing and Computer-Assisted Intervention*, pages 66–76. Springer, 2020.
26. Jure Zbontar, Li Jing, Ishan Misra, Yann LeCun, and Stéphane Deny. Barlow twins: Self-supervised learning via redundancy reduction. In *International Conference on Machine Learning*, pages 12310–12320. PMLR, 2021.
27. Hong-Yu Zhou, Chixiang Lu, Chaoqi Chen, Sibe Yang, and Yizhou Yu. A unified visual information preservation framework for self-supervised pre-training in medical image analysis. *IEEE Transactions on Pattern Analysis and Machine Intelligence*, 2023.
28. Lei Zhou, Huidong Liu, Joseph Bae, Junjun He, Dimitris Samaras, and Prateek Prasanna. Self pre-training with masked autoencoders for medical image analysis. *arXiv preprint arXiv:2203.05573*, 2022.
29. Zongwei Zhou, Md Mahfuzur Rahman Siddiquee, Nima Tajbakhsh, and Jianming Liang. Unet++: Redesigning skip connections to exploit multiscale features in image segmentation. *IEEE transactions on medical imaging*, 39(6):1856–1867, 2019.